2026 IEEE/SICE International Symposium on System Integration (SII)
January 11-14, 2026. Cancún, México

# Hybrid High-Speed Picker: Introduction of a novel hybrid Kinematic Structure

Benedikt Held[1], Christian Meierlohr[1], Frank King[1], and Franz Haas[2]

*Abstract*— **Industrial robots often perform handling and assembly tasks in industrial applications. This places high demands on dynamics and positioning accuracy. However, when handling low-weight workpieces, a relatively high robot mass usually leads to a limitation of the motion dynamics. The reason is that the manipulator's gears and drives are often arranged in series, as in the case of SCARA or articulated robots. This results in high moments of inertia for the actuated axes, located at the start of the kinematic chain. The overall stiffness is determined by the weakest element of the structure in that cases. Manipulators with parallel kinematic structures, such as delta robots, can provide a remedy here. However, when using manipulators of this type, problems arise when integrating them into production systems. They have an unfavourable ratio of workspace to installation space. Installation above the process area is mandatory and therefore strongly restricts the arrangement of other components in the production system. Hybrid structures, consisting of open and closed kinematic chains, offer alternative solutions. Based on such a hybrid approach, a concept of a novel kinematic structure for high dynamic applications is presented and analysed in this publication.**

## I. INTRODUCTION

Integration of industrial robots in industrial production systems poses a problem of varying complexities depending on the type of robot. The global market volume of industrial robots is distributed by type as follows [1]: articulated (69.8 %), SCARA (17.1 %), cartesian (10.0 %), parallel (1.0 %), and other robots (2.2 %). The high number of articulated and SCARA robots is primarily due to their ease of integration, costs, and flexibility. Robots of these types have a serial kinematic chain, which means that their gears, drives, and linkage elements are arranged sequentially. Due to the serial arrangement, these manipulators offer a large workspace in relation to their installation space and can be easily positioned beside the space where the task is to be processed (task space) via floor mounting. Considering the performance criteria for industrial robots [2], pose accuracy and pose repeatability are dependent on the rated path velocity. It can be stated that the natural frequencies of the manipulator limit its dynamics, taking into account the required accuracy. The ratio between mass and stiffness determines the natural frequencies of the system. This provides the basis for describing the performance limits of serial robots [3]: To increase the nominal speed of a serial robot, it requires an increase in stiffness or dynamics. The increase in rigidity requires a constructive stiffening of the manipulator, and the increase in dynamics requires more powerful drives. Both lead to an increase in the robot's mass to be moved, in turn requiring structural reinforcement or more powerful drives. This results in a vicious circle.

The problem can be solved with parallel kinematic structures, such as delta robots. In parallel kinematic structures, the effector is connected via at least two independent kinematic chains to a fixed base. This forms a closed kinematic chain of linkages, passive joints, and drives [4]. The drives are usually mounted to the fixed base, and their mass, therefore, is independent of the vicious circle described above. Thus, for example, higher dynamics can be achieved with the same accuracy at the effector. Since the masses of these drives have no effect on each other, they can also be designed as direct drives, which have a higher mass due to their design. As a result, the elasticities of the gears are eliminated. This approach is already mentioned in [5] for serial manipulators, which leads to an increase in the frequency of the first natural oscillations. Thus, enabling a higher bandwidth of the controller, which further results in higher dynamics at the effector. Disadvantages of parallel mechanisms, in particular that of a delta robot, are the poor ratio of workspace to installation space [6] and the complex integration in a production system. A support frame must be provided above the task space in order to mount the manipulator above the process itself. Alternative parallel kinematic approaches are described in [6] or [7]. These parallel mechanisms can also be attached via a floor mounting, facilitating integration into production systems.

As a compromise between serial and parallel structures, hybrid kinematic structures can be mentioned here, such as the serial-parallel SCARA robot [8]. These structures consist of open and closed kinematic chains. This allows the advantages of both kinematic structures to combine, depending on the individual design.

Especially in pick-and-place applications of light parts, the ratio of moving robot mass to workpiece mass is very poor, which negatively impacts the energy efficiency of such systems. One example application is the separation of lightweight parts provided as bulk material using a camera-based robot feeder system [9]. In a first step, parts that are provided as bulk material are separated by a feeder. An image of the separated parts is taken using a camera that is mounted above the feeder. The position and orientation of correctly aligned parts can then be forwarded to the robot system. The robot picks the parts and feeds them to a subsequent process step. For such a motion sequence, a

[1]Benedikt Held, Christian Meierlohr, and Frank King, Faculty of Engineering Sciences, Rosenheim Technical University of Applied Sciences, Rosenheim, Germany. E-Mail: benedikt.held@th-rosenheim.de; christian.meierlohr@th-rosenheim.de; frank.king@th-rosenheim.de

[2]Franz Haas, Head of Institute of Production Engineering, Graz University of Technology, Graz, Austria. E-Mail: franz.haas@tugraz.at

978-1-6654-5784-2/26/$31.00 ©2026 IEEE

manipulator requires three translational and one rotational degree of freedom, whereby the two remaining rotational degrees of freedom in 3D must be kept constant. This type of motion is known as Schoenflies or SCARA motion, as this represents the possible displacements of a SCARA-type robot. Consequently, SCARA robots are usually used for this bulk material separation application, as they are easy to integrate. However, they have the above-mentioned drawbacks of serial kinematic structures.

Due to this gap in the state of the art of industrial part supply applications, a new type of hybrid kinematic structure is presented in this paper. A robot based on this innovative kinematic chain is suitable for high-dynamic Schoenflies motion handling tasks since the moments of inertia are comparatively low on the actuated main axes. The kinematic structure concept is presented in Section II, with four different derived configurations. In Section III, a kinematics analysis of one of the variants is performed, solving the direct and inverse kinematics problem. Furthermore, a workspace analysis is carried out in this section using singularities of the parallel mechanism as boundary conditions. Finally, to demonstrate the feasibility of the hybrid kinematic structure, a prototype of the fully parallel mechanism has been built up, as shown in Section IV.

## II. Hybrid Kinematic Structure Concept

### A. Requirements Definition

An industrial robot with superior mechanical properties to the known mechanisms has been developed for the mentioned process of bulk material separation. As described, the manipulator must be able to realize a Schoenflies motion. This means that at least four independent actuators are required, whereby the two remaining degrees of freedom must be kept constant via mechanical constraint guides. To simplify integration into production systems, it should be possible to mount the manipulator on the floor. Lightweight parts with a mass of max. $5\,\mathrm{g}$ are to be handled, whereby the entire effector should not exceed a mass of $300\,\mathrm{g}$, to keep the distal mass of the robot appropriately small. This describes the nominal load requirement for the manipulator, allowing the fourth axis to be installed in the effector for integration reasons and thus counting towards the nominal load. The dimensions of the required workspace are determined by the application's task space, as a defined pick-up area must be fully served. In order to keep the manipulability of the effector within the workspace as continuous as possible, the workspace should be free of singularities.

### B. Structural Synthesis

The idea of the kinematic structure, already mentioned in [10], is to arrange the main axes, which are required to realize the translational degrees of freedom in such a way that their interaction with each other is as small as possible with regard to their moments of inertia. When considering an articulated robot, it can be stated that a large workspace can be achieved with a serial horizontal-mounted rotary actuator as the first axis. Consequently, the drives of an attached parallel mechanism (second and third main axes) must be arranged in such a way that their masses are located as concentric as possible in the axis of rotation of the first drive. Analogous to a cylindrical coordinate system, the parallel mechanism must then be able to move the end of the kinematic chain in two dimensions, corresponding to height and radius. For this purpose, a combination of two joint rods is suitable, which must be actuated by the second and third main axes. The necessary motion transmission can be realized via a combination of passive joints and linkages. The drives for the second and third main axes can be designed as rotary or linear drives, arranged either horizontally or vertically. This results in four types of kinematic structures, as shown in Table I. The flange of the manipulator is kept constant in two orientations by a mechanical constraint consisting of two oblique prisms. In order to be able to set the remaining orientation, a serial fourth axis is also required, which can be integrated in the flange or effector. A more elegant design would be placing the axis concentric above the first main axis and transferring the rotary motion to the effector using a telescopic shaft. As kinematic Type I shows obviously the best ratio of workspace to installation space, this type was selected to be analysed in the following section.

A fully parallel kinematic structure with similarities to the first and second type of this hybrid kinematics concept has already been published in [11]. Manipulators with coaxial drives of [6] and [7] are similar to the third type. However, it is possible to differentiate the introduced concept from all known kinematic structures based on the innovative arrangement of joints and links.

TABLE I
Hybrid Kinematic Structure Types [10]

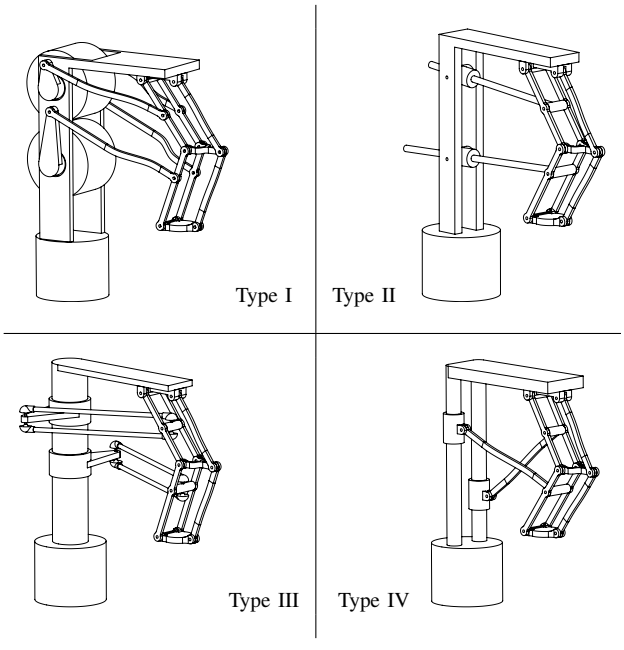

## III. Kinematic Analysis

For the Type I concept, a kinematics analysis is to be performed. The aim of this analysis is to develop a solution for the direct (DKP) and inverse (IKP) kinematics problem of the manipulator. These algorithms describe the relationship between the cartesian workspace $\underline{p} = [X \quad Y \quad Z \quad C]^{\mathrm{T}}$ and joint space $\underline{q} = [q_1 \quad q_2 \quad q_3 \quad q_4]^{\mathrm{T}}$. Where $X$, $Y$, and $Z$ describe the translational degrees of freedom of the tool center point (TCP) and $C$ the orientation around the z-axis. In joint space, the variables $q_1$ ... $q_4$ specify the positions of the actuators. Furthermore, the resulting workspace will be analysed with regard to its singularities. A schematic sketch of the kinematic structure is shown in Fig. 1. Henceforth, the

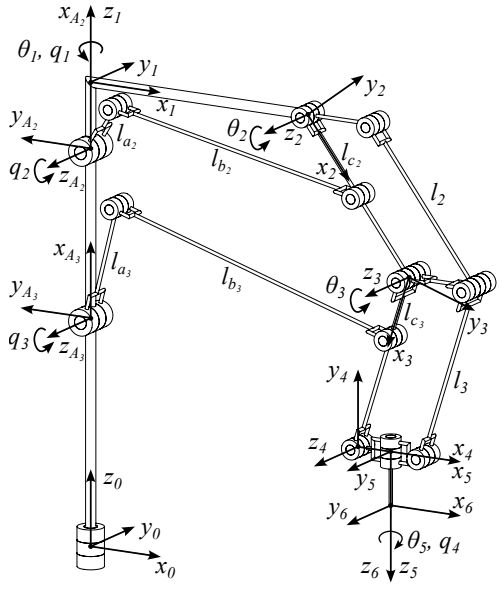


Fig. 1. Schematic sketch of the kinematic structure concept Type I.

origin of frame 6, representing the "Tool" coordinate system, is used as the location of the TCP. The kinematic dimensions of the structural elements are based on the given pick-and-place application of bulk material separation with a defined task space. The results are listed in Table II. Here, a vector ${}^{i}\underline{p}_{ik}$ describes the position of the origin of frame k from the perspective of frame i. Coordinate system $D_2$'s origin is located in frame 2, where the orientation of the $x_{D_2}$-axis is colinear with the $x_1$-axis and the $y_{D_2}$-axis is parallel to the $z_1$-axis.

### A. Direct Kinematics

To obtain the solution of the DKP, the geometric model is abstracted. First, only the serial structure of the kinematic chain is considered. The coordinate frames 0 to 6 are introduced in Fig. 1, which are arranged according to the modified Denavit-Hartenberg (DH) conventions [12]. This results in DH-parameters listed in Table III. The transformation between two coordinate frames is defined as:

$$ {}^{i-1}\underline{\underline{T}}_i = \underline{\underline{R}}_{x_{i-1},\alpha_i} \cdot \underline{\underline{D}}_{x_{i-1},a_i} \cdot \underline{\underline{R}}_{z_i,\theta_i} \cdot \underline{\underline{D}}_{z_i,d_i} \tag{1} $$

TABLE II
Kinematic Dimensions

| Vector | Dimensions (mm) |
|---|---|
| ${}^{0}\underline{p}_{01}$ | $[0 \quad 0 \quad 438]^{\mathrm{T}}$ |
| ${}^{1}\underline{p}_{12}$ | $[182.5 \quad 0 \quad 0]^{\mathrm{T}}$ |
| ${}^{4}\underline{p}_{45}$ | $[21 \quad 0 \quad 0]^{\mathrm{T}}$ |
| ${}^{5}\underline{p}_{56}$ | $[0 \quad 0 \quad 40.6]^{\mathrm{T}}$ |
| ${}^{D_2}\underline{p}_{D_2A_2}$ | $[-182.5 \quad -50 \quad 0]^{\mathrm{T}}$ |
| ${}^{D_2}\underline{p}_{D_2A_3}$ | $[-182.5 \quad -178 \quad 0]^{\mathrm{T}}$ |

| Link | Length (mm) |
|---|---|
| $l_2$ | 140 |
| $l_{a_2}$ | 40 |
| $l_{b_2}$ | 218 |
| $l_{c_2}$ | 70 |
| $l_3$ | 140 |
| $l_{a_3}$ | 90 |
| $l_{b_3}$ | 240 |
| $l_{c_3}$ | 50 |

TABLE III
Geometric Parameters from DH-Conventions

| Coordinate Frames | DH-Parameters | | | |
|---|---|---|---|---|
| | $a_i$ | $\alpha_i$ | $d_i$ | $\theta_i$ |
| 1 | 0 | 0 | ${}^{0}\underline{p}_{01,z}$ | $\theta_1$ |
| 2 | ${}^{1}\underline{p}_{12,x}$ | $\pi/2$ | 0 | $\theta_2$ |
| 3 | $l_2$ | 0 | 0 | $\theta_3$ |
| 4 | $l_3$ | 0 | 0 | $-(\theta_2+\theta_3)$ |
| 5 | ${}^{4}\underline{p}_{45,x}$ | $\pi/2$ | 0 | $\theta_5$ |
| 6 | 0 | 0 | ${}^{5}\underline{p}_{56,z}$ | 0 |

Where $\underline{\underline{D}}$ corresponds to a translation matrix and $\underline{\underline{R}}$ to a rotation matrix using homogeneous coordinates. Expanding Eq. (1) leads to the homogeneous transformation matrix [12]:

$$ {}^{i-1}\underline{\underline{T}}_i = \begin{bmatrix} \cos\theta_i & -\sin\theta_i & 0 & a_i \\ \sin\theta_i\cos\alpha_i & \cos\theta_i\cos\alpha_i & -\sin\alpha_i & -d_i\sin\alpha_i \\ \sin\theta_i\sin\alpha_i & \cos\theta_i\sin\alpha_i & \cos\alpha_i & d_i\cos\alpha_i \\ 0 & 0 & 0 & 1 \end{bmatrix} \tag{2} $$

By multiplying all transformation matrices in sequence, the entire transformation matrix can be calculated from the "World" to the "Tool" coordinate system.

$$ {}^{\mathrm{World}}\underline{\underline{T}}_{\mathrm{Tool}} = {}^{0}\underline{\underline{T}}_6 = {}^{0}\underline{\underline{T}}_1 \cdot \ldots \cdot {}^{5}\underline{\underline{T}}_6 = \begin{bmatrix} {}^{0}\underline{\underline{R}}_6 & {}^{0}\underline{p}_{06} \\ 0\,0\,0 & 1 \end{bmatrix} \tag{3} $$

The resulting passive joint angles $\theta_2$ and $\theta_3$ are to be calculated using the actuator angles $q_2$ and $q_3$. Therefore, the problem of two four-bar linkages must be solved, using a geometric approach as presented in [13]. It is demonstrated for the upper four-bar linkage in Fig. 2. To solve the problem, the coordinates of $C_2$ must be calculated with respect to frame $D_2$. Initially, calculate the vector

$$ {}^{D_2}\underline{p}_{D_2B_2} = {}^{D_2}\underline{p}_{D_2A_2} + l_{a_2} \cdot \begin{bmatrix} -\sin q_2 \\ \cos q_2 \end{bmatrix}. \tag{4} $$

This enables two circle equations to be set up, intersecting at points $C_2$ and $\overline{C_2}$. By rearranging, the quadratic equation for the x-coordinate of $C_2$ can be set up

$$ \left({}^{D_2}\underline{p}_{D_2C_2,x}\right)^2 + a \cdot \left({}^{D_2}\underline{p}_{D_2C_2,x}\right) + b = 0 \tag{5} $$

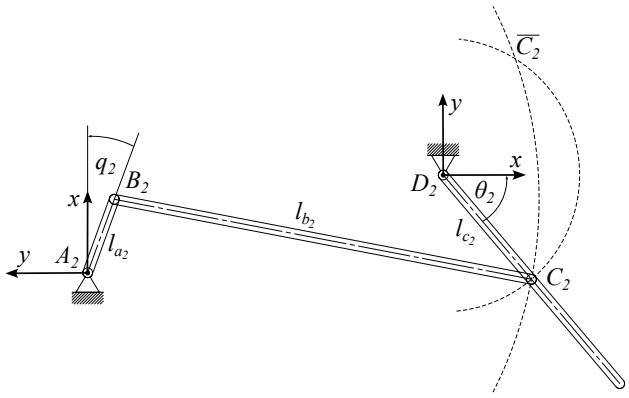


Fig. 2. Sketch of the upper four-bar linkage.

where

$$a = -\frac{2 \cdot \left({}^{D_2}\underline{p}_{D_2B_2,x}\right) \cdot L^2}{\left({}^{D_2}\underline{p}_{D_2B_2,x}\right)^2 \cdot \left({}^{D_2}\underline{p}_{D_2B_2,y}\right)^2} \tag{6}$$

$$b = \frac{L^4 - {l_{c_2}}^2 \cdot \left({}^{D_2}\underline{p}_{D_2B_2,y}\right)^2}{\left({}^{D_2}\underline{p}_{D_2B_2,x}\right)^2 \cdot \left({}^{D_2}\underline{p}_{D_2B_2,y}\right)^2} \tag{7}$$

and

$$L^2 = \frac{\left({}^{D_2}\underline{p}_{D_2B_2,x}\right)^2 \cdot \left({}^{D_2}\underline{p}_{D_2B_2,y}\right)^2 - {l_{b_2}}^2 + {l_{c_2}}^2}{2}. \tag{8}$$

If the discriminant of the quadratic equation (5) $D = 0$, there is only one intersection point, which can be referred to as a singularity, as described in Section III-C. Else if $D > 0$, two real intersection points exist. Otherwise, there is no real solution, indicating an impossible configuration of the four-bar linkage. Due to the kinematic structure, the following solution must be selected for the x-coordinate of $C_2$:

$${}^{D_2}\underline{p}_{D_2C_2,x} = -\frac{a}{2} + \sqrt{D} \tag{9}$$

Solving for the y-coordinate, the ambiguity of the root results in two additional solutions for each intersection point. Therefore, an additional criterion is needed to determine which pair of values leads to a valid configuration of the four-bar linkage. In total, up to four different value pairs can be obtained for each four-bar linkage. The required angle $\theta_2$ can be determined by

$$\theta_2 = \arctan 2\left({}^{D_2}\underline{p}_{D_2C_2,y}, {}^{D_2}\underline{p}_{D_2C_2,x}\right). \tag{10}$$

Consequently, the same solution approach can be used for the lower four-bar linkage to determine $\theta_3$, taking into account the distal position of the link $l_2$ resulting from above.

### *B. Inverse Kinematics*

In general, inverse kinematics can be obtained by an inverse transformation technique, numerical methods, or via geometric relationships. Due to the overall goal of analysing the kinematic structure, the method of geometric relationships is chosen. Calculating the actuator positions of the first vertically arranged drive axis leads to

$$q_1 = \arctan 2\left({}^{0}\underline{p}_{05,y}, {}^{0}\underline{p}_{05,x}\right). \tag{11}$$

The joint coordinate $q_4$ is the result of the difference between the cartesian orientation $C$ and $q_1$. By abstraction, only the serial kinematic chain can be considered again. So, the elbow of the manipulator can be calculated using the law of cosines, similar to serial robots [14]. The elbow, including the variables required for the calculation, is shown in Fig. 3. Using the law of cosines, the angles $\eta$ and $\xi$ can

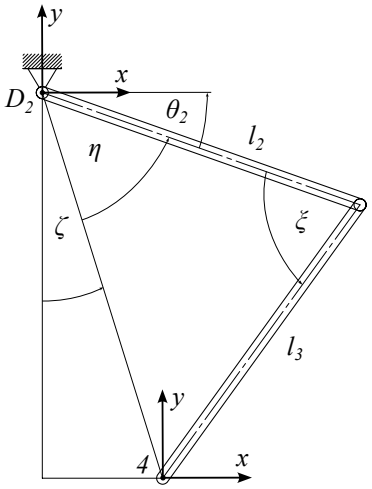


Fig. 3. Sketch of the manipulator's elbow.

be calculated:

$$\eta = \arccos\left(\frac{\left|\left|{}^{D_2}\underline{p}_{D_24}\right|\right|^2 + {l_2}^2 - {l_3}^2}{2 \cdot \left|\left|{}^{D_2}\underline{p}_{D_24}\right|\right| \cdot l_2}\right) \tag{12}$$

$$\xi = \arccos\left(\frac{{l_3}^2 + {l_2}^2 - \left|\left|{}^{D_2}\underline{p}_{D_24}\right|\right|^2}{2 \cdot l_3 \cdot l_2}\right) \tag{13}$$

Since $\cos(\varphi) = \cos(-\varphi)$, there are two solutions for $\eta$ and $\xi$. This can be explained geometrically by two possible elbow poses. However, due to the fact that a singularity-free workspace is required, a change of the elbow configuration does not have to be taken into account. By calculating

$$\zeta = \arccos\left(\frac{\left|{}^{D_2}\underline{p}_{D_24,y}\right|}{\left|\left|{}^{D_2}\underline{p}_{D_24}\right|\right|}\right), \tag{14}$$

it is possible to determine $\theta_2$ and $\theta_3$. For $\theta_2$, two different cases exist:

$$\theta_2 = \begin{cases} \eta + \zeta - \pi/2, & \text{if } \left({}^{D_2}\underline{p}_{D_24,x}\right) \geq 0 \\ \eta - \zeta - \pi/2, & \text{otherwise} \end{cases} \tag{15}$$

The four-bar linkages must now be calculated vice versa as in Section III-A to obtain the actuator positions $q_2$ and $q_3$.

As an alternative to this approach, the law of cosines or a loop closure equation can be used to find a solution.

### C. Workspace Analysis

Without considering its mechanical constraints, the usable workspace of a robot is usually restricted by singularities. These singularities can be identified using the Jacobian matrix $\underline{\underline{J}}$. The matrix $\underline{\underline{J}}$ describes the relationship between the joint velocities $\dot{\underline{q}}$ and the cartesian velocity of the effector $\dot{\underline{p}}$ in a specific robot pose [4], [15]:

$$\dot{\underline{p}} = \underline{\underline{J}}\left(\underline{q}\right) \cdot \dot{\underline{q}}, \quad \text{where} \quad \underline{\underline{J}} = \frac{\partial \underline{p}}{\partial \underline{q}}. \tag{16}$$

Furthermore, the relationship between external Forces $\underline{F}$ applied to the effector and forces/torques at the joints $\underline{\tau}$ can be described using the transpose of the Jacobian matrix [4], [12]

$$\underline{\tau} = \underline{\underline{J}}\left(\underline{q}\right)^{\mathrm{T}} \cdot \underline{F}. \tag{17}$$

According to [16], different types of singularities exist for structures with closed kinematic chains. These can be evaluated by the determinants of the Jacobian matrices $\underline{\underline{A}}$ and $\underline{\underline{B}}$, resulting from the derivative of the implicit function that describes the relationship between input and output coordinates $\underline{f}(\underline{p}, \underline{q})$ with respect to time

$$\underline{f}(\underline{p}, \underline{q}) = \underline{0}, \quad \text{thus} \quad \underline{\underline{A}} \cdot \dot{\underline{p}} + \underline{\underline{B}} \cdot \dot{\underline{q}} = \underline{0} \tag{18}$$

where

$$\underline{\underline{A}} = \frac{\partial \underline{f}}{\partial \underline{p}}, \quad \underline{\underline{B}} = \frac{\partial \underline{f}}{\partial \underline{q}}. \tag{19}$$

A classification is possible for three types of singularities, which have different physical characteristics [16]:

- Type I: $\det(\underline{\underline{B}}) = 0$ describes a singularity where an output link is at a deadpoint. In this case, the robot becomes less manipulable since the output side loses one or more degrees of freedom. Thus, movements can no longer be transmitted in certain directions.
- Type II: $\det(\underline{\underline{A}}) = 0$ describes a singularity where an input link is at a deadpoint. In this case, the output side of the robot is locally moveable even when all actuated joints are locked. This generates one or more additional degrees of freedom at the output side. Thus, forces can no longer be transmitted in certain directions.
- Type III: $\det(\underline{\underline{B}}) = \det(\underline{\underline{A}}) = 0$ describes a singularity where input and output links are at a deadpoint. In this case, a combined singularity of Type I and Type II occurs with the characteristics mentioned before. This is why this type of singularity is not explained in further detail.

In order to describe the singularities of Type I and II by an explicit Jacobian matrix, the following line of reasoning can be used.

The Type I singularity describes a pose of the manipulator in which a change in components of the vector $\underline{q}$ does not result in a change in $\underline{p}$. This can be represented by a drop in the rank of the Jacobian matrix. Thus, for $\det(\underline{\underline{J}}(\underline{q}))$ in the case of a singularity Type I, it can be concluded that

$$\det\left(\underline{\underline{J}}\left(\underline{q}\right)\right) \underset{\text{Type I}}{\longrightarrow} 0. \tag{20}$$

Unlike a Type I singularity, the Type II singularity describes a pose in which it is not possible for a component on the input side to transmit force/torque to the output side. By rearranging Eq. (17), the force generated on the output side can be represented by a function of the transposed Jacobian matrix and the actuator torques/forces

$$\underline{F} = \left(\underline{\underline{J}}\left(\underline{q}\right)^{\mathrm{T}}\right)^{-1} \cdot \underline{\tau}. \tag{21}$$

Since the output link cannot resist certain applied forces in a Type II singularity even when all actuators are locked, Eq. (22) applies:

$$\det\left(\left(\underline{\underline{J}}\left(\underline{q}\right)^{\mathrm{T}}\right)^{-1}\right) \overset{!}{=} 0 \quad \Leftrightarrow \quad \frac{1}{\det\left(\underline{\underline{J}}\left(\underline{q}\right)\right)} \overset{!}{=} 0 \tag{22}$$

So a singularity Type II can be represented by a drop in the rank of the inverse Jacobian matrix $\det(\underline{\underline{J}}(\underline{q}))^{-1}$ and this requires:

$$\det\left(\underline{\underline{J}}\left(\underline{q}\right)\right) \underset{\text{Type II}}{\longrightarrow} \infty \tag{23}$$

So both types of singularities can be described by $\det(\underline{\underline{J}}(\underline{q}))$. Since an explicit solution exists for both the DKP and the IKP, it can be concluded that an explicit solution also exists for the Jacobian matrix. Due to the parallel mechanism of the hybrid kinematic, an analytical derivation is very complex and computationally demanding. Therefore, a numerical computation method for the partial derivatives of the DKP with respect to the actuator variables is used as described in [17]. Merz [6] provides a formulation of the problem, which is used in Eq. (24). Here, $\underline{p}_i$ corresponds to the output coordinate index $i$ depending on the input coordinate vector $\underline{q}$. The vector $\delta\underline{\varepsilon}_k$ is equivalent to a vector with the same dimension as $\underline{q}$, whose component with the index $k$ has the value $\delta\varepsilon = 10^{-8}\,\mathrm{rad}$ and all others are zero.

$$\frac{\partial \underline{p}_i}{\partial \underline{q}_k} = \frac{\underline{p}_i\left(\underline{q} + \delta\underline{\varepsilon}_k\right) - \underline{p}_i(\underline{q})}{\delta\varepsilon}. \tag{24}$$

The resulting absolute values of the Jacobian matrix determinants are plotted in Fig. 4 for defined grid points in the xz-plane. Only points that are located within the area restricted by singularities are mapped. The result is the two-dimensional workspace of the fully parallel structure, completely free of singularities. Thereby, the determinant of the Jacobian matrix provides the information about the type of singularity that restricts the workspace. It can be shown that the singularity-free workspace is limited by five boundaries, whereby only the upper left boundary is defined by a singularity of Type II. The other boundaries, with the exception of two points (singularities Type III), are defined by singularities of Type I. In the neighbourhood of a Type II singularity, the effector is highly manipulable. This leads to a disadvantage with regard to the resulting position error,

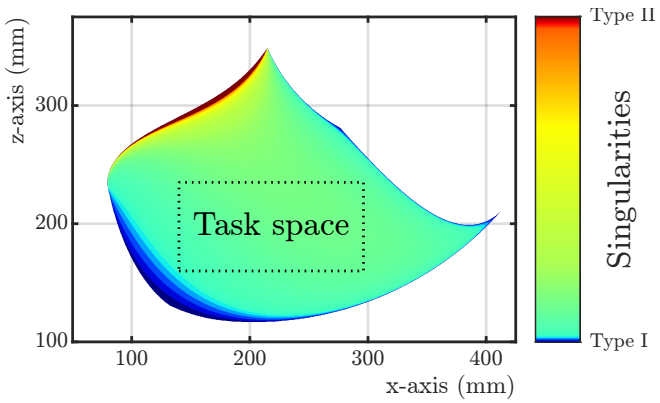


Fig. 4. Two-dimensional workspace of the parallel mechanism with characterization of singularities using the determinant of Jacobian matrix $\underline{\underline{J}}$, covering a required task space.

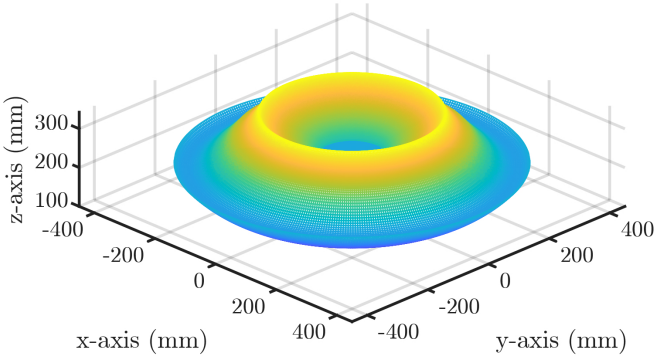


Fig. 5. Three-dimensional plot of the singularity-free workspace.

as a small actuator error causes a relatively large output-side error. Furthermore, in the neighbourhood of a Type II singularity, it must be taken into account that high actuator torque/force must be applied in order to transmit an output-side force. Consequently, the task space should be as far away as possible from any workspace boundary of Type II. As already mentioned in Section II-A, the task space is defined by a specific application. Depending on the location of the manipulator relative to the job to be processed, this results in a task space shown in Fig. 4. The task space is completely integrated in the singularity-free workspace. The balanced relationship between possible singularity-free movement space and the required task space proves that the geometric dimensions of the structural elements are appropriately designed. It can also be noted that the determinant of the Jacobian matrix is fairly constant within the task space. This leads to the conclusion that the transmission ratio of velocity and force from the actuator to the effector is nearly continuous, enabling movements without abrupt changes for precise handling tasks.

The workspace analysis is completed by a three-dimensional plot of the singularity-free workspace shown in Fig. 5. This workspace is the result of the rotation of the first serially arranged axis of the hybrid kinematic structure. The envelope curve of the two-dimensional singularity-free workspace of the fully parallel structure of Fig. 4 is thus converted into a three-dimensional envelope surface. Its shape can be described as similar to a torus, with the hole in the center later being filled by the manipulator's mechanics. This workspace covers a volume of $0.056\,\mathrm{m}^3$, without considering the mechanics of a manipulator.

## IV. Hybrid Kinematic Structure Prototype

From workspace analysis III-C, it can be concluded that the singularity-free workspace is appropriate in relation to the required application, respectively the task space. Furthermore, it can be concluded from the smooth transmission quality within the task space that the kinematic dimensions are suitable for the application. Therefore, the kinematic dimensions provided in Table II are used to realize a first functional prototype. The current status of the realized functional model is shown in Fig. 6.

The prototype is designed using a model-based development approach. To determine the load cases and required actuator torques, a multibody simulation model is set up. The trajectories for testing are based on the ADEPT-cycle, whereby the TCP is moved with a maximum acceleration of $50\,\frac{\mathrm{m}}{\mathrm{s}^2}$. The multibody simulation provides input data for mechanical dimensioning and design, like necessary actuator torques or reaction forces arising in the bearings. This allows the system to be developed mechanically in an iterative process. The linkage elements of the manipulator are made from carbon fibre reinforced plastic tubes and aluminium for high stiffness combined with low weight. As a design method for the aluminium parts, topology optimization has been used, with the intention of minimizing the element's mass required for the defined load cases from the multibody simulation. The components are connected to each other with preloaded angular contact ball bearings. As a result, the system is statically indeterminate, which means that the components are exposed to additional stresses due to manufacturing tolerances. The assembling of the components operates without the need to bend or twist the connecting elements, despite the fact that they have been produced with standard manufacturing tolerances. The actuators of the parallel mechanism are designed as direct drives and are in-house developments based on the specific requirements in terms of torque and installation space. They basically consist of a built-in torque motor, an absolute modular angle measurement device, an electromagnetic brake, and custom-made manufacturing parts. The drives have an output on both sides, which enables the swing arms to be actuated synchronously. The actuators are controlled by an industrial motion control system, with path planning being calculated by a higher-level programmable logic controller (PLC). The model-based development approach provides the direct generation of source code (e.g., DKP, IKP) for the target hardware by PLC coders.

In the following realization step, the mechanism of the fully parallel structure is to be placed on the serial first axis, resulting in a hybrid kinematic structure. An illustration of the hybrid prototype is shown in Fig. 7. The functional model

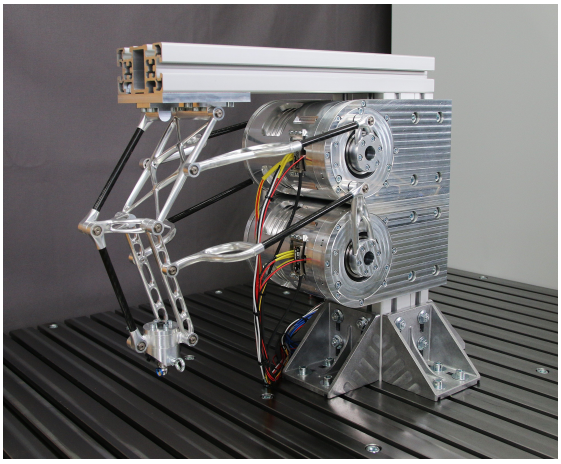

Fig. 6. Test stand of the realized prototype.

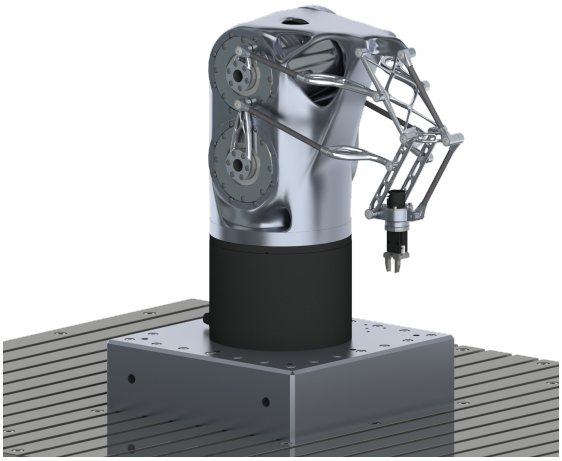

Fig. 7. Rendered CAD-model of the hybrid prototype.

is upgraded with a direct drive rotary table, a topology-optimized frame, and an effector. In order to be able to provide the necessary rotational degree of freedom for the Schoenflies motion, the effector is equipped with a rotary drive, representing the fourth actuating axis.

Measurements of performance criteria in accordance with ISO 9283 and energy consumption are planned after the prototype is realized. Further key figures to compare existing industrial robot types are related to geometric parameters. As already mentioned in Section I, parallel kinematic structures are characterized by a poor ratio of workspace to installation space. To this aspect, Merz [6] has already published investigations. Here, serial robots show a ratio higher than $1$, whereas parallel robots have a ratio below $0.6$. As part of this evaluation, the ratio of two SCARA robots ($1.1$ and $2.5$) and one delta robot ($0.2$) has been determined. According to the definitions used in [6], the installation space of the new manipulator shown in Fig. 7 covers a volume of $0.052\,\mathrm{m}^3$. This corresponds to a rectangular cuboid that encloses the manipulator in its maximum stretch pose. Taking into account the mechanical limitations of the manipulator, the workspace from Section III-C must be reduced to $0.053\,\mathrm{m}^3$. As an important benefit result, the hybrid prototype has a workspace to installation space ratio of $1.02$, equivalent to a typical SCARA robot, but enables the advantages of parallel kinematic structures to be realized.

## V. Conclusion

A novel hybrid multi-axis kinematic structure is introduced, with four different types to be elaborated. Based on this kinematic structure, the manipulator is able to realize a Schoenflies motion and allows an easy integration in production lines. Type I of this concept is analysed in detail with respect to its kinematics. Thus, explicit solutions are first developed for the DKP and IKP. A singularity-free workspace is identified, and the boundaries of this workspace are characterized based on the type of the corresponding singularities. The analysis confirms that the dimensions of the manipulator meet the requirements for the task space specified by the application. The development of a functional prototype has been started, with the parallel structure being realized first. Finally, a complete hybrid prototype is presented, that can perform a Schoenflies motion. The solution represents a novel approach that fulfils the requirements of high-speed and accurate assembling of low weight parts with less energy demand for sustainable production.

## References


[1] C. Müller, "World robotics 2024–industrial robots," IFR Statistical Department, Frankfurt am Main, Germany, Tech. Rep., 2024.

[2] *Manipulating industrial robots – Performance criteria and related test methods*, International Organization for Standardization ISO 9283, Apr. 1998.

[3] M. Frindt, "Modulbasierte Synthese von Parallelstrukturen für Maschinen in der Produktionstechnik," Ph.D. dissertation, Technische Universität Braunschweig, 2001.

[4] J.-P. Merlet, *Parallel Robots*, 2nd ed. Dordrecht, The Netherlands: Springer, 2006.

[5] W. Scholich-Tessmann, "Direktantriebe für Industrieroboter," Ph.D. dissertation, Universität Stuttgart, Stuttgart, 1998.

[6] M. Merz, "PenTec – ein neues Parallelstruktur-Konzept," Ph.D. dissertation, Technische Universität Braunschweig, 2006.

[7] M. Isaksson, K. Marlow, T. Brogårdh, and A. Eriksson, "A comparison of the yaw constraining performance of scara-tau parallel manipulator variants via screw theory," in *2016 IEEE International Conference on Robotics and Automation (ICRA)*, 2016, pp. 888–893.

[8] H. Makino, "ASSEMBLY ROBOT," U.S. Patent US4 341 502A, 1997.

[9] C. Finetto, M. Faccio, G. Rosati, and A. Rossi, "Mixed-model sequencing optimization for an automated single-station fully flexible assembly system (F-FAS)," in *The International Journal of Advanced Manufacturing Technology*, vol. 70. Springer, 2014, pp. 797–812.

[10] B. Held and C. Meierlohr, "Manipulator und Roboteraufbau," German Patent Application DE 10 2024 101 989 A1, July 24, 2025.

[11] A. Colamussi, "High-speed industrial handler," European Patent Application EP1 052 071A2, 2000, withdrawn.

[12] B. Siciliano and O. Khatib, *Springer Handbook of Robotics*, 2nd ed. Berlin Heidelberg, Germany: Springer, 2016.

[13] J. Dankert and H. Dankert, *Technische Mechanik, Statik, Festigkeitslehre, Kinematik/Kinetik*, 7th ed. Wiesbaden, Germany: Springer Vieweg, 2013.

[14] W. Weber, *Industrieroboter, Methoden der Steuerung und Regelung*, 4th ed. Munich, Germany: Hanser, 2019.

[15] P. Corke, *Robotics, Vision and Control*, 2nd ed. Cham, Switzerland: Springer International Publishing, 2017.

[16] C. Gosselin and J. Angeles, "Singularity analysis of closed-loop kinematic chains," in *IEEE Transactions on Robotics and Automation*, vol. 6, no. 3, 1990, pp. 281–290.

[17] A. Codourey, "Dynamic modelling and mass matrix evaluation of the delta parallel robot for axes decoupling control," in *Proceedings of IEEE/RSJ International Conference on Intelligent Robots and Systems. IROS '96*, vol. 3, 1996, pp. 1211–1218.